



The role of history and strength of the oceanic forcing in sea-level projections from Antarctica with the Parallel Ice Sheet Model

Ronja Reese¹, Anders Levermann^{1,2,3}, Torsten Albrecht¹, H el ene Seroussi⁴, and Ricarda Winkelmann^{1,2}

¹ Potsdam Institute for Climate Impact Research (PIK), Member of the Leibniz Association, P.O. Box 60 12 03, 14412 Potsdam, Germany

² University of Potsdam, Institute of Physics and Astronomy, Karl-Liebknecht-Str. 24-25, 14476 Potsdam, Germany

³ LDEO, Columbia University, New York, USA

⁴ Jet Propulsion Laboratory, California Institute of Technology, Pasadena, CA, USA

Correspondence: Ronja Reese (ronja.reese@pik-potsdam.de)

Abstract. Mass loss from the Antarctic Ice Sheet constitutes the largest uncertainty in projections of future sea-level rise. Ocean-driven melting underneath the floating ice shelves and subsequent acceleration of the inland ice streams is the major reason for currently observed mass loss from Antarctica and is expected to become more important in the future. Here we show that for projections of future mass loss from the Antarctic Ice Sheet, it is essential (1) to better constrain the sensitivity of sub-shelf melt rates to ocean warming, and (2) to include the historic trajectory of the ice sheet. In particular, we find that while the ice-sheet response in simulations using the Parallel Ice Sheet Model is comparable to the median response of models in three Antarctic Ice Sheet Intercomparison projects – initMIP, LARMIP-2 and ISMIP6 – conducted with a range of ice-sheet models, the projected 21st century sea-level contribution differs significantly depending on these two factors. For the highest emission scenario RCP8.5, this leads to projected ice loss ranging from 1.4 to 4.0 cm of sea-level equivalent in the ISMIP6 simulations where the sub-shelf melt sensitivity is comparably low, opposed to a likely range of 9.2 to 35.9 cm using the exact same initial setup, but emulated from the LARMIP-2 experiments with a higher melt sensitivity based on oceanographic studies. Furthermore, using two initial states, one with and one without a previous historic simulation from 1850 to 2014, we show that while differences between the ice-sheet configurations in 2015 are marginal, the historic simulation increases the susceptibility of the ice sheet to ocean warming, thereby increasing mass loss from 2015 to 2100 by about 50%. Our results emphasize that the uncertainty that arises from the forcing is of the same order of magnitude as the ice-dynamic response for future sea-level projections.



1 Introduction

Observations show that the Antarctic Ice Sheet is currently not in equilibrium and that its contribution to global sea-level rise is increasing (Shepherd et al., 2018). Its future contribution is the largest uncertainty in sea-level projections (Pörtner et al., 2019) with its evolution driven by snowfall increases (e.g., Ligtenberg et al., 2013; Frieler et al., 2015) that are counteracted by increased ocean forcing (e.g., Hellmer et al., 2012; Naughten et al., 2018) and potentially instabilities such as the Marine Ice Sheet Instability (Weertman, 1974; Schoof, 2007) and the Marine Ice Cliff Instability (DeConto and Pollard, 2016).

In recent years, sea-level projections of the Antarctic Ice Sheet were conducted with individual ice-sheet models (e.g., DeConto and Pollard, 2016; Golledge et al., 2019) and extended by comprehensive community efforts such as the Ice Sheet Model Intercomparison Project for CMIP6 (ISMIP6, Nowicki et al., 2016, in prep; Seroussi et al., under review) and the Linear Antarctic Response Model Intercomparison Project (LARMIP-2, Levermann et al., 2014, 2019) projects. In ISMIP6, a protocol for Antarctic projections was developed and ice-sheet model responses to oceanic and atmospheric forcing from selected CMIP5 models (Barthel et al., 2019) were gathered and compared for the first time. As a first step of ISMIP6, initMIP-Antarctica did test the effect of different model initialisation on idealized experiments (Seroussi et al., 2019). While the response of the ice sheet to surface mass balance forcing was similar among the models, they showed very different responses to basal melt rate changes. Similarly, in ISMIP6 a large spread in model projections is found, ranging from -7.8 to 30.0 cm of Sea-Level Equivalent (SLE) under the highest greenhouse gas emission scenario (Representative Concentration Pathway RCP8.5) with the largest uncertainties coming from ocean-induced melt rates, the calibration of melt rates and the ice dynamic response to oceanic changes. Sea-level estimates in ISMIP6 are in many cases substantially lower than the ocean-driven mass loss projected by LARMIP-2. In LARMIP-2, the sea-level contribution of the Antarctic Ice Sheet is emulated from step-forcing experiments using linear response function theory (Winkelmann and Levermann, 2013). A median mass loss of 18 cm with a likely range from 9 cm to 38 cm and a very likely range of 6 cm to 61 cm is found. In contrast to ISMIP6, atmospheric changes are not considered in LARMIP-2, and we here focus on the dynamic, ocean-driven response of the ice sheet.

In projections of the future Antarctic sea-level contribution following the ISMIP6 and LARMIP-2 protocols, oceanic forcing is obtained from sub-surface ocean conditions in general circulation models, e.g., from results of the fifth phase of the Coupled Model Intercomparison Project (CMIP5, Taylor et al., 2012). This approach takes into account that sub-shelf melt rates are mainly driven by inflow of ocean water masses at depth (Jacobs et al., 1992). However, CMIP5 models do not include ice-shelf cavities and related feedbacks that might increase the future oceanic forcing on the ice shelves (Bronselaeer et al., 2018; Golledge et al., 2019). Alternatively, output from regional models that resolve ocean dynamics on the continental shelf and within the ice-shelf cavities could be used (e.g., Hellmer et al., 2012; Naughten et al., 2018).

The sub-surface ocean forcing informs parameterisations that provide melt rates underneath the ice shelves for ice-sheet models. For the ISMIP6 experiments, a depth-dependent, non-local parameterisation and a depth-dependent, local parameterisation have been proposed (Jourdain et al., under review) that both mimic a quadratic dependency of melt rates on thermal forcing (Holland et al., 2008). As an alternative, more complex modules that capture the basic physical processes within ice-shelf cavities have been developed recently (Lazeroms et al., 2018; Reese et al., 2018). We here analyse results as submitted to



ISMIP6 that apply the Potsdam Ice-shelf Cavity mOdel (PICO; Reese et al., 2018) which extends the ocean box model (Olbers and Hellmer, 2010) for application in three-dimensional ice-sheet models. The model has been tested and compared to other parameterisations for an idealized geometry (Favier et al., 2019). In this case, the induced ice-sheet response matches the response driven by a three-dimensional ocean model. In contrast to ISMIP6, the LARMIP-2 experiments are forced by basal-melt rate changes directly. Scaling factors between global mean temperature changes and Antarctic sub-surface temperature changes are determined from CMIP5 models. These are used to generate ocean temperature forcing under different RCP scenarios emulated from MAGICC-6.0 RCP realisations (Meinshausen et al., 2011). Sub-shelf melt rates are assumed to increase by 7 to 16 m a⁻¹ per degree of sub-surface ocean warming, based on Jenkins (1991) and Payne et al. (2007). Here we compare simulations with the Parallel Ice Sheet Model as submitted to ISMIP6 with results obtained following the LARMIP-2 protocol and analyse (1) the effect of the oceanic forcing and (2) the effect of a historic simulation preceding the projections. In Sect. 2 we describe the methods used and the initial configurations of PISM. This is followed by an analysis of the experiments for ISMIP6 with only ocean forcing applied and the results obtained when following the LARMIP-2 protocol in Sect. 3. These are compared and discussed in Sect. 4 and 5.

2 Methods

We use the comprehensive, thermo-mechanically coupled Parallel Ice Sheet Model (PISM, Bueler and Brown, 2009; Winkelmann et al., 2011; the PISM authors, 2019) which employs a superposition of the Shallow-Ice and Shallow-Shelf Approximations (Hutter, 1983; Morland, 1987; MacAyeal, 1989). We apply a power law for sliding with a Mohr–Coulomb criterion relating the yield stress to parameterized till material properties and the effective pressure of the overlaying ice on the saturated till (Bueler and Pelt, 2015). Basal friction and sub-shelf melting are linearly interpolated on a sub-grid scale around the grounding line (Feldmann et al., 2014). The surface gradient in the driving stress is calculated using centered differences of the ice thickness across the grounding line. We apply eigen-calving (Levermann et al., 2012) in combination with the removal of ice that is thinner than 50 m or extends beyond present-day ice fronts (Fretwell et al., 2013).

2.1 Initial configurations

We use two model configurations of the Antarctic Ice Sheet that were submitted to ISMIP6, one with and one without a preceding historic simulation from 1850 to 2014. Both configurations share the same initialisation procedure: Starting from Bedmap2 ice thickness and topography (Fretwell et al., 2013), a spin up is run for 400,000 years with constant geometry to obtain a thermodynamic equilibrium with present-day climate on 16 km. Based on this, an ensemble of simulations for varying parameters related to basal sliding is run over 12,000 years to near steady state conditions on 8km horizontal resolution with 121 vertical layers with a quadratic spacing from 13 m at the ice shelf base to 100 m towards the surface. The initial configuration was selected from this ensemble by scoring against present-day observations of ice geometry and speed (Fretwell et al., 2013; Rignot et al., 2011). The historic simulation is based on the same initial configuration and additionally applies



atmospheric and oceanic forcing over the period from 1850 to 2015 as described below. The initial state for the experiments without historic simulation and the initial configuration after the historic simulation are shown in Fig S.1.

85 2.2 Surface mass balance

Surface mass balance and ice surface temperatures for the initial configuration without historic are from RACMOv2.3p2 (1986 to 2005 averages, Van Wessem et al., 2018), remapped from 27 km resolution. The historic simulation is started from the same conditions with historic surface mass balance and surface temperature changes following the NorESM1-M simulation as suggested by ISMIP6. Since the provided data starts in 1950, surface mass balance and temperatures are constant between
90 1850 and 1949. A new climatology for the experiments based on the historic simulation is obtained from the 1995 to 2014 average of the respective fields.

2.3 Basal mass balance

Sub-shelf melt rates are calculated by PICO that extends the ocean box model by Olbers and Hellmer (2010) for application in 3-dimensional ice sheet models (Reese et al., 2018). It mimics the vertical overturning circulation in ice-shelf cavities and
95 has two model parameters that apply for all Antarctic ice shelves simultaneously: C related to the strength of the overturning circulation and γ_T related to the vertical heat exchange across the ice-ocean boundary layer. We here use parameters $C = 1e6$ and $\gamma_T = 3 \times 10^{-5}$ that were found to yield realistic melt rates in comparison to present-day estimates (Reese et al., 2018; Rignot et al., 2013) with γ_T slightly higher than the reference value. We initialize PICO with an ocean data compilation from Locarnini et al. (2018) and Schmidtke et al. (2014). Temperatures in the Amundsen Sea had to be reduced to cold conditions
100 (-1.25°C) to prevent collapse of the region irrespective of basal sliding parameters.

Ocean temperature and salinity forcing is calculated from CMIP5 models using an anomaly approach as suggested for ISMIP6 (Barthel et al., 2019; Jourdain et al., under review). We average these values over 400 to 800 m depth to obtain suitable input for PICO. The historic forcing is based on NorESM1-M (as suggested for ISMIP6) and a new ocean climatology for the initial configuration is obtained from the 1995 to 2014 average conditions. The experiments are run using ISMIP6 ocean forcing.

105 For LARMIP-2, we add melt rate anomalies to the underlying PICO melt rates in different Antarctic regions as described in Levermann et al. (2019). Using linear response theory, the probability distribution of the sea-level contribution for RCP8.5 is then calculated following the LARMIP-2 protocol. We here exemplify the procedure for the historic configuration.

3 Results

We here present (1) the results for the two initial configurations submitted to ISMIP6 and (2) the sea-level estimates for RCP8.5
110 obtained following the LARMIP-2 and ISMIP6 experiments based on the historic configuration.

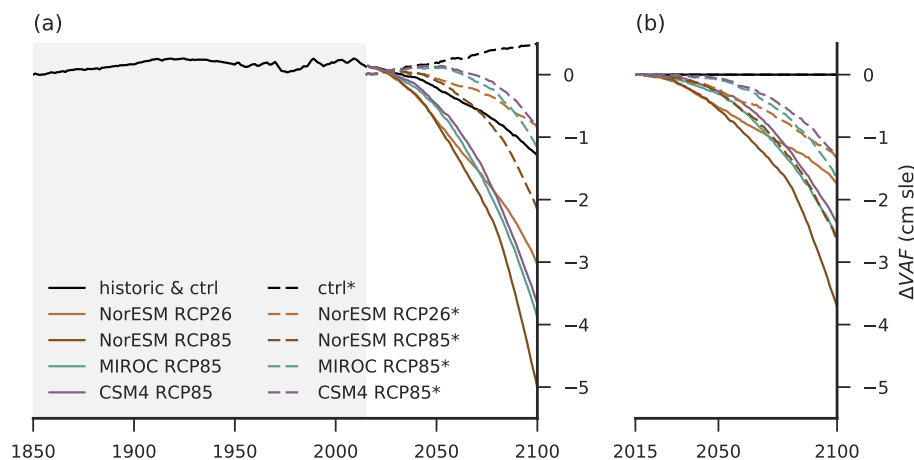


Figure 1. Mass loss of the Antarctic Ice Sheet driven by ISMIP6 ocean forcing between 2015 and 2100. Shown is the evolution of the volume above flotation (VAF) (a) relative to the start conditions and (b) with respect to the control simulations, in cm sea-level equivalent (SLE). The historic period from 1850 to 2014 is indicated by the grey background, the projection period from 2015 to 2100 by the white background. Experiments are initialized either from a historic run (solid lines) or from the initial state (dashed lines) and forced with changes in ocean temperature and salinity from the ISMIP6 experiments no. 1 to 4 with the respective CMIP5 model indicated in the legend.

3.1 Initial configurations and historic simulation

The two initial configurations for 2015, one based on a pseudo-equilibrium and one on a historic simulation from 1850 to 2014, do not differ much in terms of ice thickness, volume or speed. Over the historic period, the ice sheet thins along its margins through increased sub-shelf melting and at the same time thickens in the interior due to more snowfall.

115 These signals are smaller than 50 m over grounded regions, see also Fig. S.1. The thinning of ice shelves around the margins and subsequent reduction of buttressing causes the ice streams and ice shelves to slightly speed up over the historic simulation. These variations are smaller than the range due to parameter variations in the model ensemble. In total, the ice sheet gains mass which is equivalent to 1.6 mm of sea-level drop over the historic period, see Table 1. This mass gain over the historic simulation can be explained through the drift in the initial configuration which is 4.9 mm over 85 years (this simulation is
 120 called ctrl* in the following) which is offset by an increasing ocean forcing, see Fig. 1 and Fig. S.2.

Note that the pseudo-equilibrium simulation is not fully in equilibrium, but has a small tendency to gain mass as evident from ctrl*. In contrast, the control run started from the historic simulation (ctrl) is clearly out of equilibrium and shows a mass loss of 14.9 mm between 2015 and 2100. This change in trend is due to a net negative mass balance through the historic period with surface mass balance increased by 68 Gta^{-1} while basal mass balance increased by 420 Gta^{-1} and calving fluxes stay
 125 approximately constant. Hence total present-day mass loss (here 2014) is more realistic than starting from a pseudo-equilibrium state. Furthermore, highest mass losses are simulated in the Amundsen Sea and Totten regions which agrees with observations (Shepherd et al., 2018). Both initial configurations are further compared to other model configurations and to present-day ice thickness and velocities in Seroussi et al. (under review).



Table 1. Mass loss and evolution of surface and basal mass balance in ISMIP6 simulations.

| Experiments | ΔBMB | ΔSMB | $\Delta\text{SMB} - \Delta\text{BMB}$ | Ice mass change |
|---------------|--------------------|--------------------|---------------------------------------|-----------------|
| | Gta^{-1} | Gta^{-1} | Gta^{-1} | mm SLE |
| historic | 420 | 68 | -351 | 1.6 |
| ctrl | -8 | -17 | -9 | -14.9 |
| asmb | 21 | 747 | 726 | 104.4 |
| abmb | 531 | -68 | -599 | -57.6 |
| NorESM RCP85 | 1063 | -58 | -1121 | -54.5 |
| MIROC RCP85 | 740 | -41 | -781 | -42.5 |
| NorESM RCP26 | 99 | -39 | -138 | -33.6 |
| CCSM4 RCP85 | 782 | -47 | -829 | -40.2 |
| ctrl* | -19 | 4 | 23 | 4.9 |
| asmb* | 5 | 774 | 769 | 122.4 |
| abmb* | 543 | -52 | -595 | -34.9 |
| NorESM RCP85* | 1005 | -36 | -1041 | -22.2 |
| MIROC RCP85* | 759 | -26 | -785 | -12.1 |
| NorESM RCP26* | 60 | -21 | -81 | -8.6 |
| CCSM4 RCP85* | 768 | -24 | -792 | -8.7 |

Experiments without the historic run are indicated by *. Changes in basal and surface mass balance from the first to the last timestep in the experiments (i.e., from 1850 to 2014 in the historic run and from 2015 to 2100 in the other experiments).

3.2 Comparison to initMIP Antarctica

- 130 Results from the idealized surface mass balance experiment ‘asmb’ as described in initMIP Antarctica (Seroussi et al., 2019) are very similar for both initial states with 119 mm SLE of mass gains for the ‘historic’ configuration and 118 mm SLE for the ‘cold-start’ configuration after 85 years of simulation with respect to the control simulations, see Table 1. This is close to the response of the different models that participated in initMIP Antarctica which showed mass gains between 125 and 186 mm SLE after 100 years.
- 135 For the idealized basal melt rate experiment ‘abmb’ from initMIP Antarctica, both states are also quite similar with mass loss of 43 and 40 mm SLE after 85 years, respectively, see Table 1. In comparison, in Seroussi et al. (2019) a model spread of 13 to 427 mm SLE after 100 years is reported. Results for both configurations presented here are close to the median of model results for both experiments tested in initMIP Antarctica.

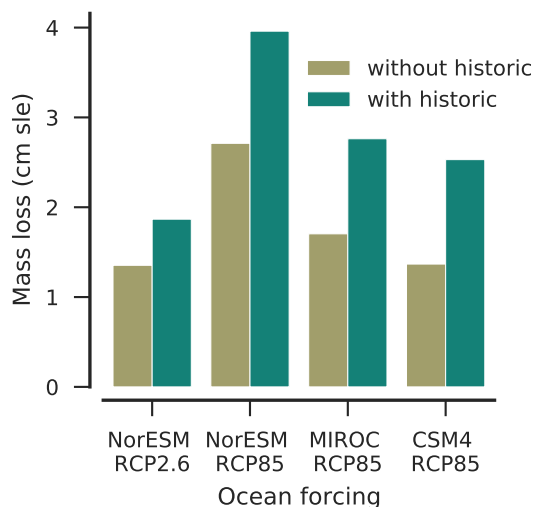


Figure 2. A preceding historic simulation increases the susceptibility of the ice sheet to ocean forcing in projections. Shown is the mass loss in simulations started directly from the initial state compared to simulations based on a historic run. The mass loss in 2100 is given with respect to the control simulation, after 85 years of applying the ocean forcing from ISMIP6 experiments no. 1 to 4 with the respective emission scenario / CMIP5 model indicated on the x-axis.

3.3 ISMIP6 ocean-forcing experiments

140 We here compare simulations for both initial configurations that are driven by ocean forcing from the ISMIP6 experiments
no. 1 to 4 (Seroussi et al., under review). The sub-surface ocean changes are obtained from the CMIP5 simulations of (1)
NorESM1-M for RCP8.5, (2) MIROC-ESM-CHEM for RCP8.5, (3) NorESM1-M for RCP2.6 and (4) CCSM4 for RCP8.5. In
general, the ice sheet's mass loss increases with stronger ocean forcing as projected for RCP8.5 in comparison to RCP2.6, see
Fig. 1. The highest losses for RCP8.5 are found for NorESM1-M. The magnitude of mass loss ranges from 1.4 to 4.0 cm SLE
145 in comparison to the control simulation, which is substantially smaller than previous estimates of Antarctica's sea-level con-
tribution from modelling studies (e.g., DeConto and Pollard, 2016; Golledge et al., 2019) or expert judgement (Bamber et al.,
2019). Furthermore, we find that the historic simulation makes the configuration more susceptible to ocean forcing, see Fig. 2.
Ocean-driven mass loss in comparison to the control run is increased by about 50% when starting from the historic simulation
in contrast to the 'cold-start'.

150 3.4 LARMIP-2 basal melt rate forcing experiments

In LARMIP-2, sea-level probability distributions from the Antarctic Ice Sheet are derived using linear response functions
as described in Levermann et al. (2019). The response functions are derived from experiments in which constant basal melt
rate forcing is applied for five different regions of Antarctica. We here perform the same experiments for both configurations
described in Sect. 2.

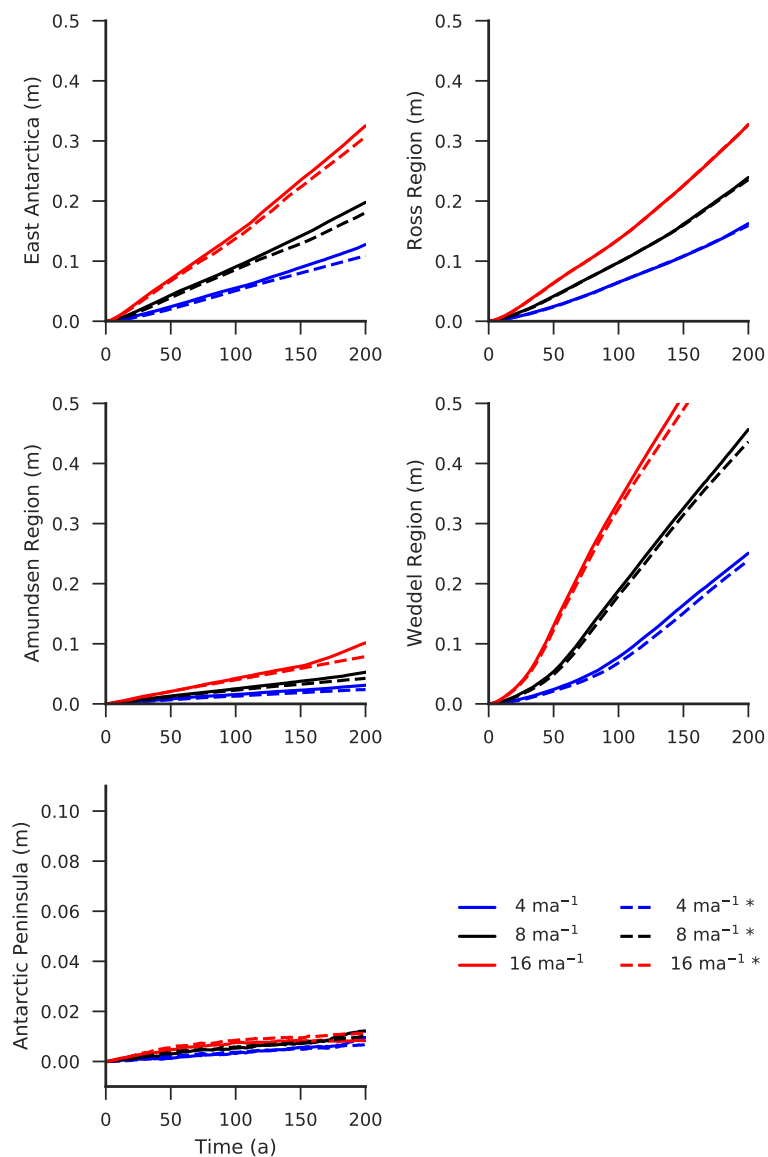


Figure 3. Mass loss of the different regions in Antarctica (indicated on y-axis) driven by constant LARMIP-2 basal melt rate forcing. For the experiments from the LARMIP-2 protocol we show the changes in volume above flotation initialized from a historic simulation (solid line) and from the initial state directly (dashed line, indicated by *). Mass loss is shown relative to the respective control simulation. From the response of the ice sheet to a constant melt rate forcing over 200 years, a response function is derived which serves then to emulate the sea-level contribution under various climate scenarios. This figure is similar to Fig. 4 in Levermann et al. (2019).

155 We find that for all regions the ice sheet response compares with the responses found in LARMIP-2 as, for example, in the PISM-PIK contribution that is based on a different initial state with 4 km horizontal resolution and that does not apply subgrid



Table 2. Percentiles of the probability distribution of the sea level contribution from Antarctica for the ISMIP6 configuration under the RCP-8.5 climate scenario ('historic' configuration).

| percentile | cm SLE |
|------------|--------|
| 5.0 % | 3.4 |
| 16.6 % | 9.2 |
| 50.0 % | 18.4 |
| 83.3 % | 35.9 |
| 95.0 % | 55.1 |

Mass loss from 2015 to 2100.

melting, compare Fig. 3 with Fig. 4 from Levermann et al. (2019). Similar to the ISMIP6 simulations, the experiments show different responses for the two initial configurations, especially in the Weddell Sea, East Antarctica and the Amundsen Sea region. The overall difference is smaller than in the ISMIP6 experiments for the stronger forcing applied here.

160 Following the procedure in LARMIP-2, we derive response functions from the idealized experiments for the five Antarctic regions, here exemplified for the 'historic' configuration. We then convolve the response function with basal melt rate forcing, given in Fig. 4, to obtain a probability distribution of the future sea-level contribution for RCP8.5 which is given in Fig. 5. The ocean-driven mass loss from 2015 to 2100 has a very likely range of 3.4 to 55.1 cm SLE, a likely range of 9.2 to 35.9 cm SLE and a median of 18.4 cm SLE (5 to 95%, 16.6 to 83.3%, and 50% percentiles, respectively, see Table 2). In comparison, the
165 PISM-PIK contribution of LARMIP-2 has a very likely range of 7 to 48 cm SLE, a likely range of 11 to 31 cm SLE and a median of 19 cm SLE for the 21st century. The resulting sea-level probability distribution is hence in line with the estimates presented in LARMIP-2.

4 Discussion

In the following, we compare the results found in the ISMIP6 and LARMIP-2 experiments, discuss the role of the ocean forcing
170 and of the historic simulation.

4.1 Comparison of LARMIP-2 and ISMIP6 sea-level projections

The projected mass loss in LARMIP-2 is an order of magnitude larger than the ocean-driven mass loss in our ISMIP6 experiments for RCP8.5, see Sect. 3. In order to understand this difference better, we here investigate the ocean forcing in more detail. We thereby focus on the RCP8.5 simulation based on NorESM1-M which shows highest mass losses of all ISMIP6
175 experiments presented in this study.

Both intercomparison projects, ISMIP6 and LARMIP-2, are based on CMIP5 model sub-surface ocean temperature changes (Levermann et al., 2014; Barthel et al., 2019; Jourdain et al., under review). While minor differences in ocean forcing might occur due to different processing steps, a more significant difference is that the LARMIP-2 experiments are driven by basal

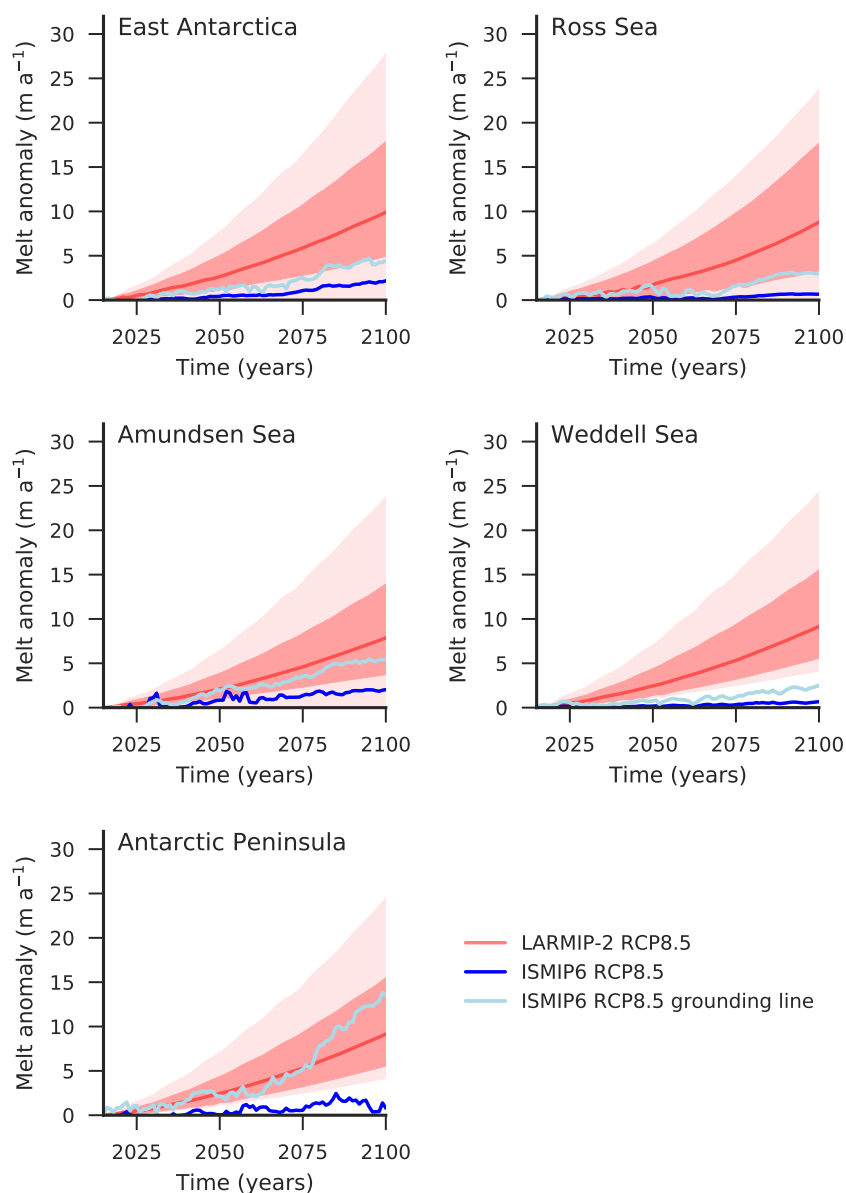


Figure 4. Projected basal melt rate changes in the different Antarctic regions from LARMIP-2 and in the ISMIP6 contribution forced with NorESM1-M ocean changes under RCP8.5. In LARMIP-2 spatially constant basal melt rate forcing is applied with corresponding very-likely ranges (5 to 95%-percentiles, light red shading), likely ranges (66%-percentile around the median, dark red shading) and median (red line) for the RCP8.5 scenario. In the ISMIP6 contribution, basal melt rates are calculated by PICO, which shows higher increases close to the grounding line (PICO Box 1, light blue lines) than averaged over the ice shelves (dark blue lines). Figure is similar to Fig. 3 in Levermann et al. (2019).

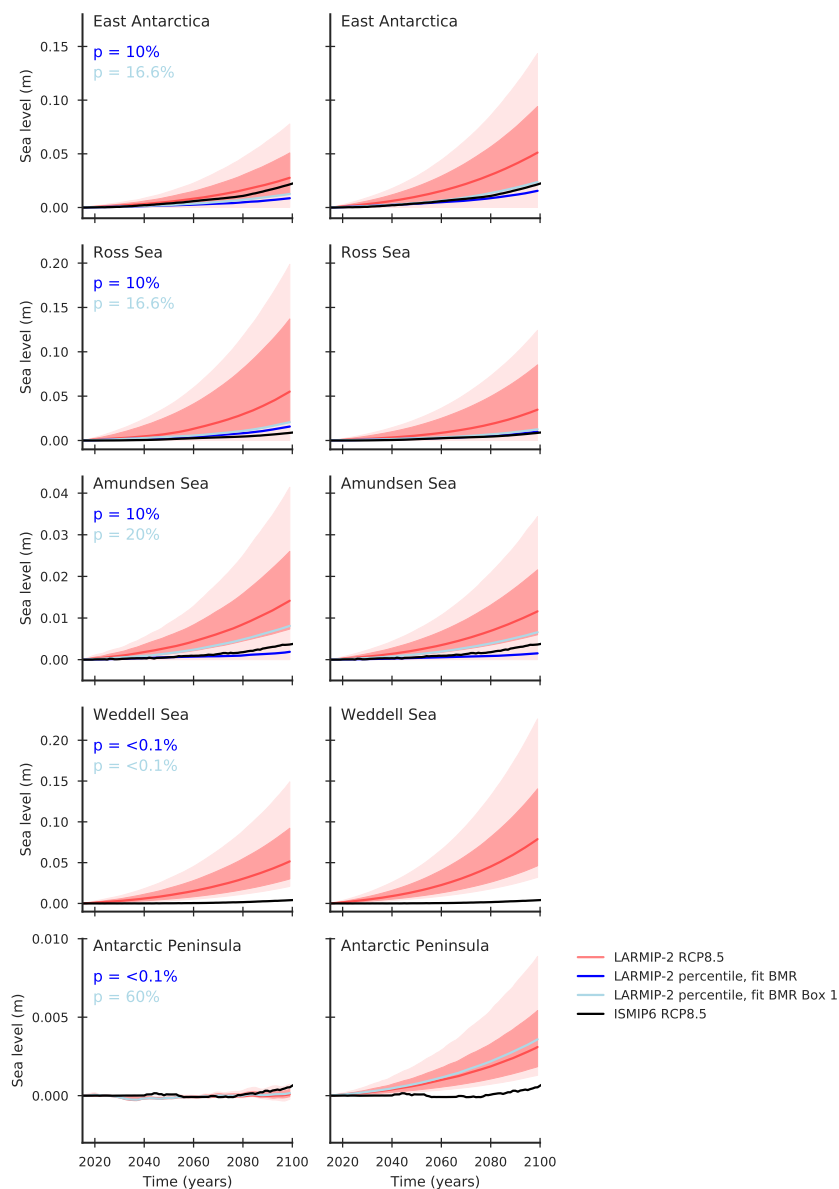


Figure 5. Projections of Antarctica’s sea level contribution under the RCP8.5 climate scenario for the different Antarctic regions for LARMIP-2 and for the ISMIP6 experiment driven by NorESM1-M ocean changes. The very likely ranges (5 to 95%-percentiles, light red shading), likely ranges (16.6 to 83.3%-percentiles, dark red shading) and the respective median (50%-percentile, red lines) of mass loss is shown for (left panels) the PISM-PIK simulations submitted to LARMIP-2 and, for comparison, (right panels) estimated following LARMIP-2 for the setup as submitted to ISMIP6. The sea-level contribution in ISMIP6 (black curve) is compared to percentiles of LARMIP-2 results which have consistent basal melt rate changes in the corresponding region close to the grounding line (light blue) or averaged over the ice shelves (dark blue line), see also Fig. 4. Corresponding percentiles are indicated in the left panels.



180 melt rate changes emulated from the forcing while in the ISMIP6 simulations ocean forcing is translated into basal melt rates via sub-shelf melt parameterisations, in our case PICO.

Figure 4 shows projected basal melt rates and their uncertainty ranges for RCP8.5 used in LARMIP-2 together with the basal melt rate changes in the ISMIP6 simulation. Note that LARMIP-2 assumes constant changes in basal melt rates over the entire ice shelf. In contrast, since PICO mimics the vertical overturning circulation in ice-shelf cavities, basal melt rates in the ISMIP6 simulation increase strongest along the grounding line (in PICO's first box) and less towards the ice shelf front. The melt rate 185 changes in PICO along the grounding line are hence an upper limit for the comparison to the LARMIP-2 forcing while the shelf-wide averaged changes provide a lower limit. Overall, we find that in the ISMIP6 simulation, basal-melt rates increase more in regions with smaller ice shelves than in the Ross and Weddell sea. Furthermore, we find that the basal melt rate changes in our ISMIP6 contribution in all Antarctic regions is located in the lower range (percentiles) of the LARMIP-2 forcing. Only for the Antarctic Peninsula, PICO melt rates along the grounding line increase stronger than the median in LARMIP-2. For all 190 other regions, melt rate changes along the grounding line are smaller than the median in LARMIP-2 (50%-percentile). For the Amundsen Sea region, they lie within the likely range (16.6% to 83.3% percentiles), for East Antarctica and the Ross Sea, they are around the lower margin of the likely range and for the Weddell Sea, they are lower than the very likely range (5% to 95% percentiles). Shelf-wide changes are generally smaller than the likely range, for the Weddell Sea and the Antarctic Peninsula they are also smaller than the very likely range.

195 This is consistent with the mass loss in the ISMIP6 simulation being lower than the likely range of LARMIP-2 for almost all regions, see Fig. 5. Based on the comparison of basal melt rate changes above, we identify for each region two percentiles from the LARMIP-2 basal melt probability distribution: the first percentile reflects the changes along the grounding line and the second the changes averaged over the entire ice shelf. When comparing the corresponding percentiles of mass loss in LARMIP-2 (derived for the same initial configuration) with the ISMIP6 simulation, we find that indeed the changes at the 200 grounding line provide an upper limit while the changes over the entire ice shelf provide a lower limit for the actual mass loss. No valid comparison can be made in the Weddell Sea, where the basal melt rate forcing is lower than the 0.1%-percentile from LARMIP-2, and for the shelf-wide average forcing at the Antarctic Peninsula, where mass loss is generally low. These findings are underlined by comparison with the PISM-PIK contribution to LARMIP-2 which is based on a different initial setup. Overall, we find that mass losses in the ISMIP6 projections are generally lower than the likely range in LARMIP-2 and 205 in the Weddell Sea, losses are smaller than the very likely range.

4.2 Role of ocean forcing and basal melt rate sensitivity

In order to gain a better understanding of the conversion of ocean forcing to basal melt rates in LARMIP-2 and in our ISMIP6 contribution, we analyse the sensitivity to ocean warming.

We perform step-forcing experiments for both initial configurations for ISMIP6 and diagnose the effect on basal melt rates in 210 PICO, see Fig. 6. We find that the sensitivity in the Amundsen Sea Region is comparatively high with about $10 \text{ ma}^{-1}\text{K}^{-1}$, while the sensitivity in the Weddell Sea is lower with about $1.5 \text{ ma}^{-1}\text{K}^{-1}$, which yields for the entire Antarctic ice shelves an overall sensitivity of about $2.2 \text{ ma}^{-1}\text{K}^{-1}$. The sensitivities for melting close to the grounding line are as expected a bit

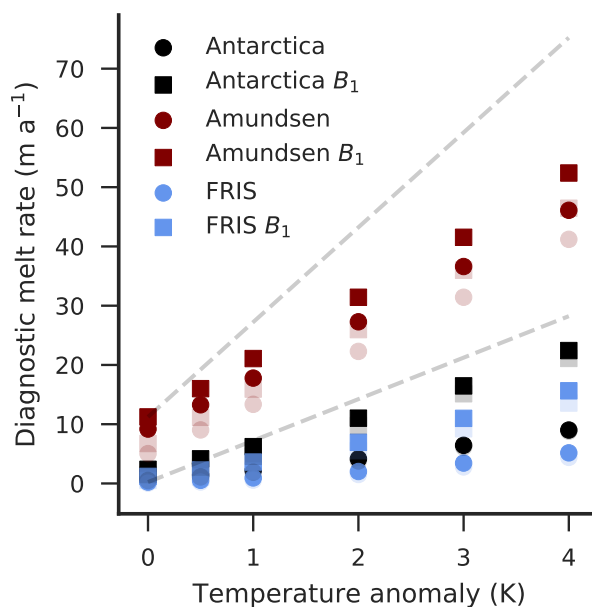


Figure 6. Sensitivity of basal melt rates to ocean temperatures in PICO. Diagnosed from the historic configuration (solid) and the cold-start configuration (shaded) in 2015 using step-wise ocean temperature increases. Dots show shelf-wide averages while boxes indicate the basal melt rates close to the grounding lines (in PICO box B_1). The dashed grey lines indicate the sensitivity estimates used in Levermann et al. (2019).

higher: $10.5 \text{ ma}^{-1}\text{K}^{-1}$ for the Amundsen Sea region, $3.9 \text{ ma}^{-1}\text{K}^{-1}$ for the Weddell Sea and $5.3 \text{ ma}^{-1}\text{K}^{-1}$ for all Antarctic ice shelves. In both cases, the Antarctic-wide sensitivity is substantially lower than the sensitivity used in LARMIP-2. In the latter study, a sensitivity between 7 and $16 \text{ ma}^{-1}\text{K}^{-1}$, based on Jenkins (1991) and Payne et al. (2007), is assumed to translate ocean forcing into sub-shelf melt rates. This is consistent with our findings in the previous section that in the ISMIP6 simulations mass loss from the Antarctic Ice Sheet, and especially from the regions that drain the large Filchner-Ronne and Ross ice shelves, is smaller than the likely range estimated following the LARMIP-2 protocol. Jourdain et al. (under review) report that a different tuning of the ISMIP6 basal melt parameterisation to fit observations in the Amundsen Sea (from Dutrieux et al., 2014; Jenkins et al., 2018) substantially increases the sensitivity to ocean changes and Seroussi et al. (2019) find that this enhances the sea-level contribution by a factor of six.

Since the sensitivity in PICO depends on the parameters used, with the overturning coefficient C affecting the sensitivity in large ice shelves and the heat exchange coefficient γ_T affecting the sensitivity in small ice shelves, a different tuning could improve basal melt rate sensitivities and thereby lead to higher mass losses in the ISMIP6-experiments. This would however affect the comparison of sub-shelf melt rates to present-day observations, see Fig. 4 in Reese et al. (2018). One approach could be to introduce additional degrees of freedom through temperature corrections for the ice shelves that reflect uncertainties in ocean properties, as for example used in Lazeroms et al. (2018) and Jourdain et al. (under review).



230 Few observations exist for targeted tuning of the sensitivity of basal melt rate parameterizations to ocean temperatures, hence the use of dynamic modelling of the ocean circulation in ice-shelf cavities could be explored. Note that we provided linear estimates of the sensitivity in the discussion above, while Holland et al. (2008) report a quadratic dependency of melt rates on thermal forcing. They also discuss that the sensitivity depends on ice shelf cavity properties such as the slope of the ice-shelf draft and shape of the ice shelf and that sensitivities are generally higher close to the grounding line.

4.3 Role of historic trajectory of the Antarctic Ice Sheet

235 We find that while the historic simulation has no large effect on the initial sea-level volume (the overall difference being 1.6 mm SLE), it strongly affects the mass loss in the projections. One reason might be that the initial state switches from close-to steady state to a state that is out of balance with a tendency to mass loss. Also, the grounding line retreats during the historic simulation slightly into deeper regions, where the local freezing point at the ice shelf base near the grounding line is decreased due to its pressure dependence. Hence more heat is available for melting the ice-shelf base, which shows also in an increased sensitivity to ocean changes, see Fig. 6. In particular for lower temperatures, PICO shows a non-linear sensitivity of melt rates to ocean 240 temperatures, as discussed in Reese et al. (2018).

5 Conclusions

In this study we compare sea-level projections for RCP8.5 from the Antarctic Ice Sheet as submitted to ISMIP6 and projections derived following the LARMIP-2 protocol, both using the Parallel Ice Sheet Model. Overall, we find that the sea-level contribution driven by ocean forcing in ISMIP6 is smaller than the likely range of the sea-level probability distribution in 245 LARMIP-2. This difference can be explained by the comparably low sensitivity of melt rates to ocean temperature changes for the parameter tuning in the basal-melt rate module PICO as used for the ISMIP6 simulations here. Future sea-level projections should hence carefully consider the sensitivity of basal melt rates to ocean changes. Further observations in combination with ocean modelling are needed to better constrain this sensitivity for the diverse ice-shelf cavities in Antarctica. Furthermore, we find that while including the historic evolution starting in 1850 has very little effect on the simulated current ice mass or ge- 250 ometry, it increases the projected mass loss in 2100 by about 50%. This means that not only the currently committed sea-level contribution should be considered in projections, but also the effect of the historic forcing on the ice sheet's susceptibility to ocean changes. Hence, further investigations are needed to assess the sensitivity of basal melting to ocean temperatures for basal-melt parameterizations and the role of historic forcing in future sea-level projections.

255 *Code and data availability.* Data and code is available from the authors upon request. Model outputs from the simulations for ISMIP6 described in this paper will be made available via the ISMIP6 project with digital object identifier. The PISM code as well as the scripts to analyse the simulations and create the figures will be made available with digital object identifier reference.



Competing interests. Helene Seroussi is an editor of the special issue The Ice Sheet Model Intercomparison Project for CMIP6 (ISMIP6). The authors declare that no other competing interests are present.

Acknowledgements. We thank the Climate and Cryosphere (CliC) effort, which provided support for ISMIP6 through sponsoring of work-
260 shops, hosting the ISMIP6 website and wiki, and promoted ISMIP6. We acknowledge the World Climate Research Programme, which, through its Working Group on Coupled Modelling, coordinated and promoted CMIP5. We thank the climate modeling groups for producing and making available their model output, the Earth System Grid Federation (ESGF) for archiving the CMIP data and providing access, the University at Buffalo for ISMIP6 data distribution and upload, and the multiple funding agencies who support CMIP5 and ESGF. We thank the ISMIP6 steering committee, the ISMIP6 model selection group and ISMIP6 dataset preparation group for their continuous en-
265 gagement in defining ISMIP6. This is ISMIP6 contribution No X. Development of PISM is supported by NASA grant NNX17AG65G and NSF grants PLR-1603799 and PLR-1644277. The authors gratefully acknowledge the European Regional Development Fund (ERDF), the German Federal Ministry of Education and Research and the Land Brandenburg for supporting this project by providing resources on the high performance computer system at the Potsdam Institute for Climate Impact Research. Computer resources for this project have been also provided by the Gauss Centre for Supercomputing/Leibniz Supercomputing Centre (www.lrz.de) under Project-ID pr94ga and pn69ru.
270 R.R. is supported by the Deutsche Forschungsgemeinschaft (DFG) by grant WI4556/3-1. T.A. is supported by the Deutsche Forschungsgemeinschaft (DFG) in the framework of the priority program “Antarctic Research with comparative investigations in Arctic ice areas” by grant WI4556/2-1 and WI4556/4-1. H.S. was supported by grants from NASA Cryospheric Science and Modeling, Analysis, Predictions Programs.



References

- 275 Bamber, J. L., Oppenheimer, M., Kopp, R. E., Aspinall, W. P., and Cooke, R. M.: Ice sheet contributions to future sea-level rise from structured expert judgment, *Proceedings of the National Academy of Sciences*, 116, 11 195–11 200, 2019.
- Barthel, A., Agosta, C., Little, C. M., Hatterman, T., Jourdain, N. C., Goelzer, H., Nowicki, S., Seroussi, H., Straneo, F., and Bracegirdle, T. J.: CMIP5 model selection for ISMIP6 ice sheet model forcing: Greenland and Antarctica, *The Cryosphere Discuss.*, <https://doi.org/10.5194/tc-2019-191>, 2019.
- 280 Bronselaer, B., Winton, M., Griffies, S. M., Hurlin, W. J., Rodgers, K. B., Sergienko, O. V., Stouffer, R. J., and Russell, J. L.: Change in future climate due to Antarctic meltwater, *Nature*, 564, 53, 2018.
- Bueler, E. and Brown, J.: Shallow shelf approximation as a “sliding law” in a thermomechanically coupled ice sheet model, *Journal of Geophysical Research*, 114, <https://doi.org/10.1029/2008JF001179>, 2009.
- Bueler, E. and Pelt, W. v.: Mass-conserving subglacial hydrology in the Parallel Ice Sheet Model version 0.6, *Geoscientific Model Development*, 8, 1613–1635, 2015.
- 285 DeConto, R. M. and Pollard, D.: Contribution of Antarctica to past and future sea-level rise, *Nature*, 531, 591, 2016.
- Dutrioux, P., De Rydt, J., Jenkins, A., Holland, P. R., Ha, H. K., Lee, S. H., Steig, E. J., Ding, Q., Abrahamsen, E. P., and Schröder, M.: Strong sensitivity of Pine Island ice-shelf melting to climatic variability, *Science*, 343, 174–178, 2014.
- Favier, L., Jourdain, N. C., Jenkins, A., Merino, N., Durand, G., Gagliardini, O., Gillet-Chaulet, F., and Mathiot, P.: Assessment of sub-shelf
- 290 melting parameterisations using the ocean–ice–sheet coupled model NEMO (v3. 6)–Elmer/Ice (v8. 3), *Geoscientific Model Development*, 12, 2255–2283, 2019.
- Feldmann, J., Albrecht, T., Khroulev, C., Pattyn, F., and Levermann, A.: Resolution-dependent performance of grounding line motion in a shallow model compared with a full-Stokes model according to the MISIP3d intercomparison, *Journal of Glaciology*, 60, 353–360, <https://doi.org/doi:10.3189/2014JoG13J093>, 2014.
- 295 Fretwell, P., Pritchard, H. D., Vaughan, D. G., Bamber, J. L., Barrand, N. E., Bell, R., Bianchi, C., Bingham, R. G., Blankenship, D. D., Casassa, G., Catania, G., Callens, D., Conway, H., Cook, A. J., Corr, H. F. J., Damaske, D., Damm, V., Ferraccioli, F., Forsberg, R., Fujita, S., Gim, Y., Gogineni, P., Griggs, J. A., Hindmarsh, R. C. A., Holmlund, P., Holt, J. W., Jacobel, R. W., Jenkins, A., Jokat, W., Jordan, T., King, E. C., Kohler, J., Krabill, W., Riger-Kusk, M., Langley, K. A., Leitchenkov, G., Leuschen, C., Luyendyk, B. P., Matsuoka, K., Mouginot, J., Nitsche, F. O., Nogi, Y., Nost, O. A., Popov, S. V., Rignot, E., Rippin, D. M., Rivera, A., Roberts, J., Ross, N., Siegert, M. J.,
- 300 Smith, A. M., Steinhage, D., Studinger, M., Sun, B., Tinto, B. K., Welch, B. C., Wilson, D., Young, D. A., Xiangbin, C., and Zirizzotti, A.: Bedmap2: improved ice bed, surface and thickness datasets for Antarctica, *The Cryosphere*, 7, 375–393, <https://doi.org/10.5194/tc-7-375-2013>, 2013.
- Frieler, K., Clark, P. U., He, F., Buizert, C., Reese, R., Ligtenberg, S. R., Van Den Broeke, M. R., Winkelmann, R., and Levermann, A.: Consistent evidence of increasing Antarctic accumulation with warming, *Nature Climate Change*, 5, 348, 2015.
- 305 Golledge, N. R., Keller, E. D., Gomez, N., Naughten, K. A., Bernaldes, J., Trusel, L. D., and Edwards, T. L.: Global environmental consequences of twenty-first-century ice-sheet melt, *Nature*, 566, 65, 2019.
- Hellmer, H. H., Kauker, F., Timmermann, R., Determann, J., and Rae, J.: Twenty-first-century warming of a large Antarctic ice-shelf cavity by a redirected coastal current, *Nature*, 485, 225, 2012.
- Holland, P. R., Jenkins, A., and Holland, D. M.: The Response of Ice Shelf Basal Melting to Variations in Ocean Temperature, *Journal of*
- 310 *Climate*, 21, 2558–2572, <https://doi.org/10.1175/2007JCLI1909.1>, 2008.



- Hutter, K. E.: Theoretical Glaciology; Material Science of Ice and the Mechanics of Glaciers and Ice Sheets, 1983.
- Jacobs, S., Hellmer, H., Doake, C. S. M., Jenkins, A., and Frolich, R. M.: Melting of ice shelves and the mass balance of Antarctica, *Journal of Glaciology*, 38, 375–387, <https://doi.org/10.3189/S0022143000002252>, 1992.
- Jenkins, A.: Ice shelf basal melting: Implications of a simple mathematical model, *Filchner-Ronne Ice Shelf Programme Report*, 5, 32–36, 315 1991.
- Jenkins, A., Shoosmith, D., Dutriex, P., Jacobs, S., Kim, T. W., Lee, S. H., Ha, H. K., and Stammerjohn, S.: West Antarctic Ice Sheet retreat in the Amundsen Sea driven by decadal oceanic variability, *Nature Geoscience*, 11, 733, 2018.
- Jourdain, N. C., Asay-Davis, X. S., Hattermann, T., Straneo, F., Seroussi, H., Little, C. M., and Nowicki, S. M. J.: Ocean forcing for the ISMIP6 Antarctic ice sheet projections, *The Cryosphere Discuss.*, pp. 1–33, <https://doi.org/10.5194/tc-2019-277>, under review.
- 320 Lazeroms, W. M. J., Jenkins, A., Gudmundsson, G. H., and van de Wal, R. S. W.: Modelling present-day basal melt rates for Antarctic ice shelves using a parametrization of buoyant meltwater plumes, *The Cryosphere*, 12, 49–70, <https://doi.org/10.5194/tc-12-49-2018>, <https://www.the-cryosphere.net/12/49/2018/>, 2018.
- Levermann, A., Albrecht, T., Winkelmann, R., Martin, M. A., Haseloff, M., and Joughin, I.: Kinematic first-order calving law implies potential for abrupt ice-shelf retreat, *The Cryosphere*, 6, 273–286, 2012.
- 325 Levermann, A., Winkelmann, R., Nowicki, S., Fastook, J. L., Frieler, K., Greve, R., Hellmer, H. H., Martin, M. A., Meinshausen, M., Mengel, M., Payne, A. J. J., Pollard, D., Sato, T., Timmermann, R., Wang, W. L. L., and Bindschadler, R. A. A.: Projecting Antarctic ice discharge using response functions from SeaRISE ice-sheet models, *Earth System Dynamics*, 5, 271–293, 2014.
- Levermann, A., Winkelmann, R., Albrecht, T., Goelzer, H., Golledge, N. R., Greve, R., Huybrechts, P., Jordan, J., Leguy, G., Martin, D., Morlighem, M., Pattyn, F., Pollard, D., Quiquet, A., Rodehacke, C., Seroussi, H., Sutter, J., Zhang, T., Van Breedam, J., DeConto, R., 330 Dumas, C., Garbe, J., Gudmundsson, G. H., Hoffman, M. J., Humbert, A., Kleiner, T., Lipscomb, W., Meinshausen, M., Ng, E., Perego, M., Price, S. F., Saito, F., Schlegel, N.-J., Sun, S., and van de Wal, R. S. W.: Projecting Antarctica’s contribution to future sea level rise from basal ice-shelf melt using linear response functions of 16 ice sheet models (LARMIP-2), *Earth System Dynamics Discussions*, 2019, 1–63, <https://doi.org/10.5194/esd-2019-23>, <https://www.earth-syst-dynam-discuss.net/esd-2019-23/>, 2019.
- Ligtenberg, S., Van de Berg, W., Van den Broeke, M., Rae, J., and Van Meijgaard, E.: Future surface mass balance of the Antarctic ice sheet 335 and its influence on sea level change, simulated by a regional atmospheric climate model, *Climate dynamics*, 41, 867–884, 2013.
- Locarnini, R., Mishonov, A., Baranova, O., Boyer, T., Zweng, M., Garcia, H., J.R. Reagan, a. D. S., Weathers, K., Paver, C., and Smolyar, I.: *World Ocean Atlas 2018, Volume 1: Temperature.*, <https://www.nodc.noaa.gov/OC5/woa18/woa18data.html>, NOAA Atlas NESDIS in preparation, 2018.
- MacAyeal, D. R.: Large-scale ice flow over a viscous basal sediment: Theory and application to ice stream B, Antarctica, *Journal of Geo- 340 physical Research: Solid Earth*, 94, 4071–4087, 1989.
- Meinshausen, M., Raper, S. C., and Wigley, T. M.: Emulating coupled atmosphere-ocean and carbon cycle models with a simpler model, *MAGICC6–Part 1: Model description and calibration*, *Atmospheric Chemistry and Physics*, 11, 1417–1456, 2011.
- Morland, L. W.: *Unconfined Ice-Shelf Flow*, pp. 99–116, Springer Netherlands, Dordrecht, https://doi.org/10.1007/978-94-009-3745-1_6, 1987.
- 345 Naughten, K. A., Meissner, K. J., Galton-Fenzi, B. K., England, M. H., Timmermann, R., and Hellmer, H. H.: Future projections of Antarctic ice shelf melting based on CMIP5 scenarios, *Journal of Climate*, 31, 5243–5261, 2018.
- Nowicki, S. et al.: ISMIP6-Protocol paper, *The Cryosphere*, in prep.



- Nowicki, S. M. J., Payne, A., Larour, E., Seroussi, H., Goelzer, H., Lipscomb, W., Gregory, J., Abe-Ouchi, A., and Shepherd, A.: Ice Sheet Model Intercomparison Project (ISMIP6) contribution to CMIP6, *Geoscientific Model Development*, 9, 4521–4545, <https://doi.org/10.5194/gmd-9-4521-2016>, 2016.
- 350 Olbers, D. and Hellmer, H.: A box model of circulation and melting in ice shelf caverns, *Ocean Dynamics*, 60, 141–153, <https://doi.org/10.1007/s10236-009-0252-z>, 2010.
- Payne, A. J., Holland, P. R., Shepherd, A. P., Rutt, I. C., Jenkins, A., and Joughin, I.: Numerical modeling of ocean-ice interactions under Pine Island Bay’s ice shelf, *Journal of Geophysical Research: Oceans*, 112, <https://doi.org/10.1029/2006JC003733>, c10019, 2007.
- 355 Pörtner, H.-O., Roberts, D., Masson-Delmotte, V., Zhai, P., Tignor, M., Poloczanska, E., Mintenbeck, K., Nicolai, M., Okem, A., Petzold, J., Rama, B., and Weyer, N. e.: IPCC, 2019: Summary for Policymakers. In: IPCC Special Report on the Ocean and Cryosphere in a Changing Climate, 2019.
- Reese, R., Albrecht, T., Mengel, M., Asay-Davis, X., and Winkelmann, R.: Antarctic sub-shelf melt rates via PICO, *The Cryosphere*, 12, 1969–1985, 2018.
- 360 Rignot, E., Mouginot, J., and Scheuchl, B.: Ice flow of the Antarctic ice sheet, *Science*, 333, 1427–1430, 2011.
- Rignot, E., Jacobs, S., Mouginot, J., and Scheuchl, B.: Ice-shelf melting around Antarctica., *Science*, 341, 266–270, <https://doi.org/10.1126/science.1235798>, 2013.
- Schmidtko, S., Heywood, K. J., Thompson, A. F., and Aoki, S.: Multidecadal warming of Antarctic waters, *Science*, 346, 1227–1231, <https://doi.org/10.1126/science.1256117>, 2014.
- 365 Schoof, C.: Marine ice-sheet dynamics. Part 1. The case of rapid sliding, *Journal of Fluid Mechanics*, 573, 27–55, 2007.
- Seroussi, H., Nowicki, S., Simon, E., Abe-Ouchi, A., Albrecht, T., Brondex, J., Cornford, S., Dumas, C., Gillet-Chaulet, F., Goelzer, H., et al.: initMIP-Antarctica: an ice sheet model initialization experiment of ISMIP6, *The Cryosphere*, 13, 1441–1471, 2019.
- Seroussi, H. et al.: ISMIP6-Antarctica: results, *The Cryosphere*, under review.
- Shepherd, A., Ivins, E., Rignot, E., Smith, B., Van Den Broeke, M., Velicogna, I., Whitehouse, P., Briggs, K., Joughin, I., Krinner, G., et al.: Mass balance of the Antarctic Ice Sheet from 1992 to 2017, *Nature*, 558, 219–222, 2018.
- 370 Taylor, K. E., Stouffer, R. J., and Meehl, G. A.: An Overview of CMIP5 and the Experiment Design, *Bulletin of the American Meteorological Society*, 93, 485–498, <https://doi.org/10.1175/BAMS-D-11-00094.1>, 2012.
- the PISM authors: PISM, a Parallel Ice Sheet Model, <http://www.pism-docs.org>, 2019.
- Van Wessem, J. M., Jan Van De Berg, W., Noël, B. P., Van Meijgaard, E., Amory, C., Birnbaum, G., Jakobs, C. L., Krüger, K., Lenaerts, J., Lhermitte, S., et al.: Modelling the climate and surface mass balance of polar ice sheets using RACMO2: Part 2: Antarctica (1979–2016), *Cryosphere*, 12, 1479–1498, 2018.
- Weertman, J.: Stability of the junction of an ice sheet and an ice shelf, *Journal of Glaciology*, 13, 3–11, 1974.
- Winkelmann, R. and Levermann, A.: Linear response functions to project contributions to future sea level, *Climate dynamics*, 40, 2579–2588, 2013.
- 380 Winkelmann, R., Martin, M. A., Haseloff, M., Albrecht, T., Bueller, E., Khroulev, C., and Levermann, A.: The Potsdam Parallel Ice Sheet Model (PISM-PIK) – Part 1: Model description, *The Cryosphere*, 5, 715–726, <https://doi.org/10.5194/tc-5-715-2011>, 2011.